The Determination of Anisotropic and Nonlinear Properties of Rock through Triaxial and Hydrostatic Testing

Ian Gray[a*], Xiaoli Zhao[a], Lucy Liu[a]
[a] *Sigra Pty Ltd, Brisbane, Australia*
* ian@sigra.com.au

Abstract

Rock stiffness is important in design as it affects the stresses and deformation around openings. Many rocks are anisotropic and those of sedimentary origin are frequently highly nonlinearly elastic. Traditionally elastic properties are inadequately measured using uniaxial test methods. This paper examines the results of uniaxial, triaxial and hydrostatic testing for the elastic behaviour of rock based on the assumption of orthotropic behaviour. The effects of fluid pressure on effective stress are also discussed. The mathematics are presented for each case. The testing methods involve step-wise loading of triaxial or hydrostatic samples that are fitted with strain gauges. The effects of fluids on deformation are determined by gas injection. The simple hydrostatic test process enables rock fragments to be tested to determine their anisotropy. This however requires an estimation of at least one of the values of Poisson's ratio.

Keywords: Young's moduli, Poisson's ratios, Triaxial, Hydrostatic

Introduction

Rocks are complex composites of different minerals. As a consequence their mechanical properties are highly variable. This variability extends through varying elastic to post elastic behaviour.

For a general elastic solid there are six stresses and six engineering strains which are linked by either a compliance (Equation 1) or stiffness matrix, each with 36 terms. Because of the symmetry of these matrixes the number of terms may be reduced to 21. Practically this is still a very large number of parameters to determine from a physical test on a piece of rock, particularly as this piece of rock is frequently a cylindrical core or more conveniently a fragment.

$$\{\varepsilon_{ij}\} = [C_{ijkl}]\{\sigma_{kl}\} \quad (1)$$

The general formulation of Equation 1 means that quite complex effects can be accounted for. For example a normal stress to a plane may cause a shear strain in that same plane. More realistically shear stress acting on a plane may lead to strain (dilation or compaction) perpendicular to the plane.

If we make the convenient, but not necessarily correct, approximation that the rock behaves in an orthotropic manner, then the number of independent terms in the compliance matrix drops from 21 to nine (allowing for symmetry) as shown in Equation 2. Three of these are shear terms that are difficult to measure directly, but may be estimated. The orthotropic approach does however mean that the options such as dilation or compaction perpendicular to the plane on which shearing acts are assumed to be zero.

Practically the application of tractions to a rock sample surface is difficult to achieve. Rock may only be conveniently loaded perpendicularly to its surfaces. A core may therefore have differing axial and radial (confining) loading. The combination of these two leads to a subset of the true triaxial loading situation with equal stress being applied to the core sides, perpendicular to the core axis. This constitutes the normal triaxial loading that is available for rock core in a laboratory. The uniaxial test is a further subset of this but without any radial loading.

A non-uniform fragment of rock may be practically loaded by point loading, with an associated complex, and unanalysable, stress distribution. Alternatively it may be loaded by hydrostatic pressure, which produces an even stress distribution. These practical restrictions on testing mean that the number of parameters that may be adjusted is limited. The measurements that can be made are also limited to deformation of the surface of the rock sample being tested. The best measurements are made using strain gauges located on the surface of the sample.

$$\begin{Bmatrix} \varepsilon_{11} \\ \varepsilon_{22} \\ \varepsilon_{33} \\ \gamma_{23} \\ \gamma_{31} \\ \gamma_{12} \end{Bmatrix} = \begin{bmatrix} \frac{1}{E_1} & -\frac{\nu_{21}}{E_2} & -\frac{\nu_{31}}{E_3} & 0 & 0 & 0 \\ -\frac{\nu_{12}}{E_1} & \frac{1}{E_2} & -\frac{\nu_{32}}{E_3} & 0 & 0 & 0 \\ -\frac{\nu_{13}}{E_1} & -\frac{\nu_{23}}{E_2} & \frac{1}{E_3} & 0 & 0 & 0 \\ 0 & 0 & 0 & \frac{1}{G_{23}} & 0 & 0 \\ 0 & 0 & 0 & 0 & \frac{1}{G_{31}} & 0 \\ 0 & 0 & 0 & 0 & 0 & \frac{1}{G_{12}} \end{bmatrix} \begin{Bmatrix} \sigma_{11} \\ \sigma_{22} \\ \sigma_{33} \\ \tau_{23} \\ \tau_{31} \\ \tau_{12} \end{Bmatrix} \quad (2)$$

If we obtain core with an axis which is in the same direction as one of the principal axes of orthogonality then we have further simplified the problem of determining material properties.

Such core would typically be drilled perpendicularly to the bedding plane of a sedimentary rock, or to the laminations of a schist. If the core axis corresponds to the 1 axis of Equation 2 then it can be loaded in this direction using the axial loading platens and without any shear stresses acting on the contact surface. The radial or confining stress loading is symmetric about the 1 axis and thus no shear stresses are generated on any plane that is perpendicular to it. This means that all of the shear stress terms on the right hand side of Equation 2 disappear. By determining the principal strains in the 2-3 plane any shear strains also disappear. This means that for practical purposes the compliance matrix of Equation 2 is reduced to a symmetric 3×3 matrix with six unknowns.

To solve the components of the compliance matrix in a cylindrical triaxial test there are two load change steps (axial and radial) that can be made. Associated with these are three principal strains, albeit we have assumed that one of these principal strains is in the axis of the core and the others are perpendicular to this. This is an inadequate number from which to derive a solution and a further assumption must be made to obtain a solution.

If we consider the hydrostatic loading case then we only have a single loading change available and therefore two assumptions must be made to solve the six unknowns of the compliance matrix.

In addition to the effects of external stress on the deformation of a rock sample there are also the effects of internal fluid pressure to consider. These poroelastic effects can be measured.

1. Solutions for the components of the compliance matrix in terms of E_i and ν_{ij}

To be able determine rock properties it is necessary to measure both stress and associated strain change at a variety of stress states.

An important component of a solution to the orthogonal case comes from symmetry of the compliance matrix. This means that there is a relationship between Poisson's ratios and the Young's moduli given in Equation 3.

$$\frac{\nu_{ij}}{E_i} = \frac{\nu_{ji}}{E_j} \quad (3)$$

Another key assumption that must be used is that a geometric mean Poisson's ratio exists as given in Equation 4 in which ν_a is assumed to be common for all values of *i* and *j*.

$$\nu_{ij}\nu_{ji} = \nu_a^2 \quad (4)$$

A consequence of Equations 3 and 4 is Equation 5.

$$\nu_{ji} = \sqrt{\frac{E_j}{E_i}}\nu_a \quad (5)$$

1.1 Cylindrical triaxial case

In the case of triaxially loaded core two loading options exist: one for loading the core axially and one for loading the core radially. Both axial strain and circumferential strain may be monitored by strain gauges. The axial Young's modulus, E_1, may be directly determined by the change in axial strain associated with a change in axial stress. By measuring the circumferential strains at three points on the circumference of the sample it is possible to calculate the principal strains in the plane perpendicular to the core (2-3) and from this the values of Poisson's ratio associated with this loading, ν_{12} and ν_{13}.

Determining the other values of Young's moduli and Poisson's ratios is more complex because the cylinder is loaded radially. Equation 6 is the basic equation for strain brought about by principal stresses in an orthogonal system.

$$\Delta\varepsilon_{ii} = \frac{1}{E_i}\Delta\sigma_{ii} - \frac{v_{ji}}{E_j}\Delta\sigma_{jj} - \frac{v_{ki}}{E_k}\Delta\sigma_{kk} \tag{6}$$

Using the relationship of Equation 3 it may be rewritten as Equation 7.

$$E_i = \frac{1}{\Delta\varepsilon_{ii}}(\Delta\sigma_{ii} - v_{ij}\Delta\sigma_{ji} - v_{ik}\Delta\sigma_{kk}) \tag{7}$$

Further using the Equation 5 and Equation 7 it may be re-written in residual as Equation 8.

$$residual = fn(E_i) = \frac{1}{\Delta\varepsilon_{ii}}\left(\Delta\sigma_{ii} - \sqrt{\frac{E_i}{E_j}}v_a\Delta\sigma_{jj} - \sqrt{\frac{E_i}{E_k}}v_a\Delta\sigma_{kk}\right) - E_i \tag{8}$$

Equation 8 represents three nonlinear equations for the Young's moduli, E_i, using an unknown geometric mean value of Poisson's ratio, v_a. However the geometric mean Poisson's ratio may be deduced by solving these equations to arrive at the best fit to the directly measured value of E_1using an axial load change at the appropriate stress level. The authors have used a Newton-Raphson approach to obtain the best solution to the experimental data from each change of stress.

1.2 The hydrostatic case

In the case of hydrostatic loading there is no direct measurement of E_1 or any other value of Young's modulus or Poisson's ratio, and the value of the geometric mean Poisson's ratio, v_a, must be estimated. If this is done then the solutions for E_i are obtained by solving Equation 8, but using a single hydrostatic value of stress change rather than the three individual stress values. Using the estimated value of $v_a$it is possible to calculate the individual values of Poisson's ratios using Equation 5.

1.3 The measurement of poroelastic behaviour

Rock which contains interconnected void space will change its dimension to some degree with changing fluid pressure. How the rock deforms is a function of its elastic properties, the fluid pressure change and the poroelastic parameters. The basis for measuring the poroelastic parameters is presented in Equation 9, taken from Gray, 2017.

$$\begin{bmatrix} \frac{1}{E_1} & -\frac{v_{21}}{E_2} & -\frac{v_{31}}{E_3} \\ -\frac{v_{12}}{E_1} & \frac{1}{E_2} & -\frac{v_{32}}{E_3} \\ -\frac{v_{13}}{E_1} & -\frac{v_{23}}{E_2} & \frac{1}{E_3} \end{bmatrix} \begin{Bmatrix} \alpha_1 \\ \alpha_2 \\ \alpha_3 \end{Bmatrix} = \begin{Bmatrix} (\frac{1}{E_1}\Delta\sigma_{11} - \frac{v_{21}}{E_2}\Delta\sigma_{22} - \frac{v_{31}}{E_3}\Delta\sigma_{33} - \Delta\varepsilon_{11})/\Delta P \\ (-\frac{v_{12}}{E_1}\Delta\sigma_{11} + \frac{1}{E_2}\Delta\sigma_{22} - \frac{v_{32}}{E_3}\Delta\sigma_{33} - \Delta\varepsilon_{22})/\Delta P \\ (-\frac{v_{13}}{E_1}\Delta\sigma_{11} - \frac{v_{23}}{E_2}\Delta\sigma_{22} + \frac{1}{E_3}\Delta\sigma_{33} - \Delta\varepsilon_{33})/\Delta P \end{Bmatrix} \tag{9}$$

The elastic parameters, E_i and v_{ij} are normally solved by a regime of varied axial and radial loading on a core. During this test cycle fluid pressure is increased, the associated strains measured, and then the fluid is drained off. The poroelastic parameter tensor, α_{i}, may be deduced from the strain changes associated with the fluid pressure change.

1.4 The shear stiffness terms

Determining the shear moduli, G_{ij}, in Equation 2 is not easy because of the loading limitations on core and rock fragments. Huber (1923) took the approach shown in Equation 10 for this purpose.

$$G_{ij} = \frac{\sqrt{E_i E_j}}{2(1+\sqrt{\nu_{ij}\nu_{ji}})} \tag{10}$$

2. Experimental procedures

Three experimental procedures are considered here. They are triaxial loading, usually with fluid pressurisation, Hydrostatic loading, usually without fluid pressurisation, and uniaxial testing. The latter is included as it is so often regarded as the benchmark for the determination of rock properties.

2.1 Triaxial testing of cylindrical core

The triaxial testing of core involves preparing the sample with flat parallel ends and with plaster filling of the core periphery wherever the surface roughness would cause problems for strain gauge adherence or lead to squeezing of the gauge foil into pores. Three strain gauge rosettes are then adhered at 120^o separations around the periphery of the core. The core is then fitted into the triaxial test rig and the strain gauges are electrically coupled. A core sample is shown in this position in Figure 1. An elastomeric sleeve is then fitted over the sample and the cell is then closed ready for loading. The load is applied in a sequence of steps over a number of cycles.

Figure 1. Showing a fine grained silty sandstone core fitted with strain gauge rosettes within the triaxial cell prior to the sleeve being fitted

The first cycle involves a step increase in axial load followed by a step increase in radial loading to a fraction (typically 90%) of the axial load. This process is repeated with multiple loading increments. The system is then unloaded and a second cycle is then repeated but with the radial loading fraction at a lower value (typically 75%) of the axial load change. Additional loading cycles are undertaken with reduced radial to axial loading fractions (typically 50% and 25%). Finally a uniaxial loading cycle is performed.

The reason for starting with a loading regime where the radial load is close to the axial load is to minimise the potential for shear failure to occur early in the test process. As the test cycles proceed the potential for shear failure to occur increases.

The determination of poroelastic behaviour involves the pressurisation of the sample with gas. The gas usually used is nitrogen though helium is preferable where there is a risk of adsorbing gas into the rock material. The pressure used must be less than the radial (confining) pressure so that the gas does

not cause the elastomeric sleeve to be lifted. It is also kept at as low a pressure as is compatible with obtaining a satisfactory strain reading. Sometimes the gas injection must be maintained for a significant period to ensure permeation through the sample. By monitoring the strain gauges it is possible to determine when the strain change has stopped occurring.

Figure 2 shows a typical loading cycle for a triaxial test.

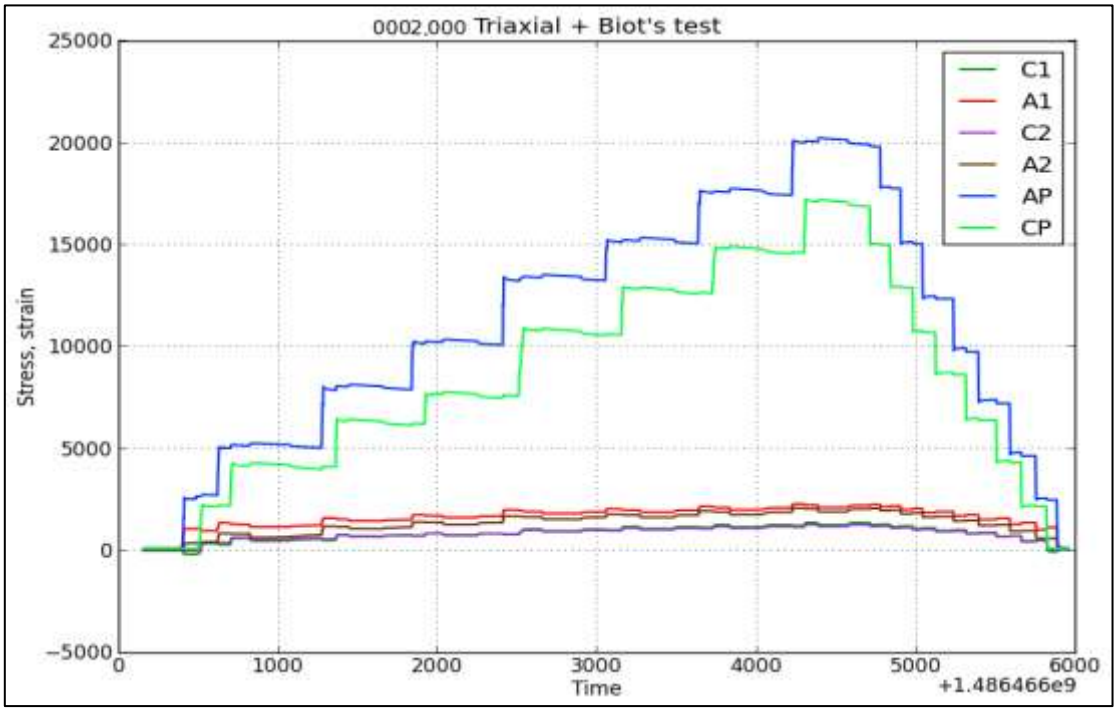

Figure 2. Example of the first cycle of stepwise axial pressure (AP) and confining pressure (CP) in kPa changes and the resulting strains in microstrain.

2.2 Hydrostatic testing of rock fragments

It is frequently impossible to obtain a suitable sample of a rock to be tested triaxially, and testing must be undertaken on a fragment. This fragment should be fitted with strain gauge rosettes. It is convenient to orient these so that they match any particular direction of anisotropy that can be observed. Once the gauges are fitted the sample is then cast in an elastomeric resin which is then allowed to set. Figure 3 shows such a sample. The strain gauge leads are then connected and the sample is sealed in a vessel which is fluid filled and pressurised in a series of pressure steps. Because the resin used is very much less stiff than the rock sample, the hydrostatic load is directly transferred to the rock surface.

2.3 Uniaxial testing

Uniaxial testing is used to such an extent that it cannot be ignored. It is a subset of the triaxial test procedure but without either radial stress or any fluid pressure. The sample is still fitted with strain gauges but loading is purely axial. Because there is no confining stress the sample will fail at a lower stress than would otherwise be the case. Indeed the uniaxial compressive strength is an important rock parameter. If only a loading Young's modulus, E_1, and Poisson's ratios, v_{12} and v_{13}, are sought then the sample can be loaded to failure. However if the unloading modulus is also sought then a number of loading and unloading cycles are required. This cyclic process avoids taking the sample to failure before unloading occurs. Figure 4 shows the results of cyclic loading on Hawkesbury sandstone. As can be seen the sample displays quite non-linear behaviour. In addition the transverse strain becomes large with considerable permanent strain, particularly circumferential strain, as the test progresses. Such behaviour is quite typical of these rocks.

Figure 3. A hydrostatic sample fitted with rosettes and cast in silicone resin. Note the bedding of the phyllite sample which is at an angle to the core.

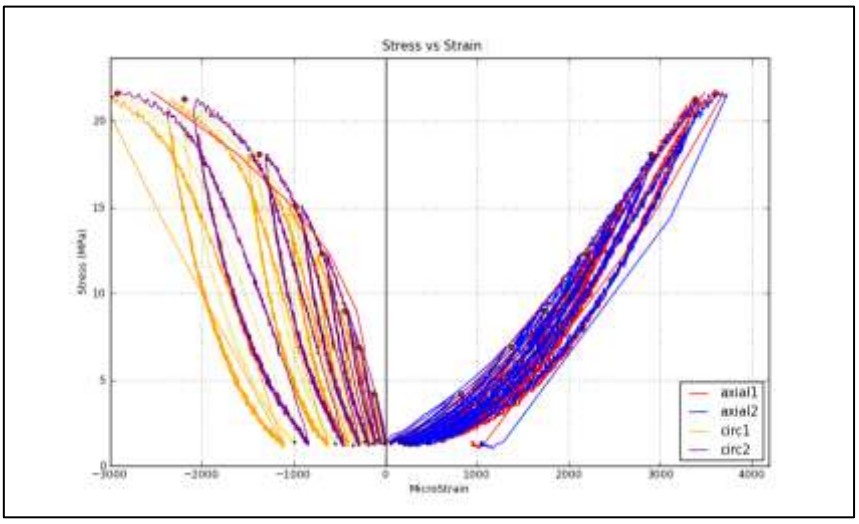

Figure 4. Results of cyclic loading of a uniaxial specimen. The x-axis shows the axial (+ve) and circumferential strain (-ve) while the y-axis shows the uniaxial stress

There are three forms of axial Young's modulus that may be determined from such a test. The first is the tangent modulus, which is defined as the slope of the axial stress vs strain plot taken between loading peaks. The second is the secant modulus which is defined as the difference between the stress at a loading peak and the stress at the start of the loading cycle (approximately zero) divided by the strain change. The unloading modulus is defined as the difference between the peak load stress and the stress at unloading (approximately zero) divided by the strain change on unloading. The loading and unloading secant Young's moduli are the same if no permanent strain occurs through the loading and unloading cycle.

There are three different Poisson's ratios corresponding to tangent, loading secant and unloading secant Young's moduli. It is only possible to compare the tangent values between the three types of test because the hydrostatic and triaxial tests are not simple unloading tests, and the loading regime is complex.

3. Experimental results

Two sets of experimental results are discussed. The first is from a fine grained, laminated, silty sandstone. The second set of experimental results comes from a test on a medium grained sample of Hawkesbury sandstone that exhibited some obvious porosity.

3.1 A fine grained silty sandstone

This sample from Permian strata of the Bowen Basin, Queensland, is shown in Figure 1. It is notable because it was first tested triaxially, then it was removed from the triaxial cell and retested uniaxially in a universal test machine. It was then drilled with a 26 mm hole in line with its axis and re-tested under uniaxial loading. Finally the central section of drilled specimen containing the strain gauges was cut out. This sample was then tested hydrostatically. The reason for drilling a hole in the specimen was to copy the geometry of an overcore stress measurement sample (Gray et al, 2013). In all cases the strain gauges were left in place.

The triaxial testing included a uniaxial cycle and gas injection for poroelastic parameter determination. Figure 6 to Figure 8 show the results of this testing as isopachs of E_1, E_3 and v_a. Figure 6 includes the values of axial Young's modulus obtained from plain axial loading of the solid core. Figure 6 and Figure 7 contain the values of Young's moduli E_1 and E_3 respectively, obtained from both triaxial and hydrostatic test processes. The results of this have been calculated using the values of v_a from triaxial testing. This is somewhat of an artificial process as a hydrostatic test would not normally be conducted on a sample that had been triaxially tested. More normally a hydrostatic test would be conducted on a short core or a fragment with an estimate of Poisson's ratio.

The sample is notable because the major horizontal to vertical stiffness ratio lies in the range of 2:1 and 3:1.

Pressurisation of the sample with gas led to negligible strain change, indicating that the poroelastic parameters were essentially zero.

The axial Young's modulus, E_1, and the average of axial Poisson's ratio derived from axial loading of the solid and hollow sample were identical within experimental error (Figure 5).

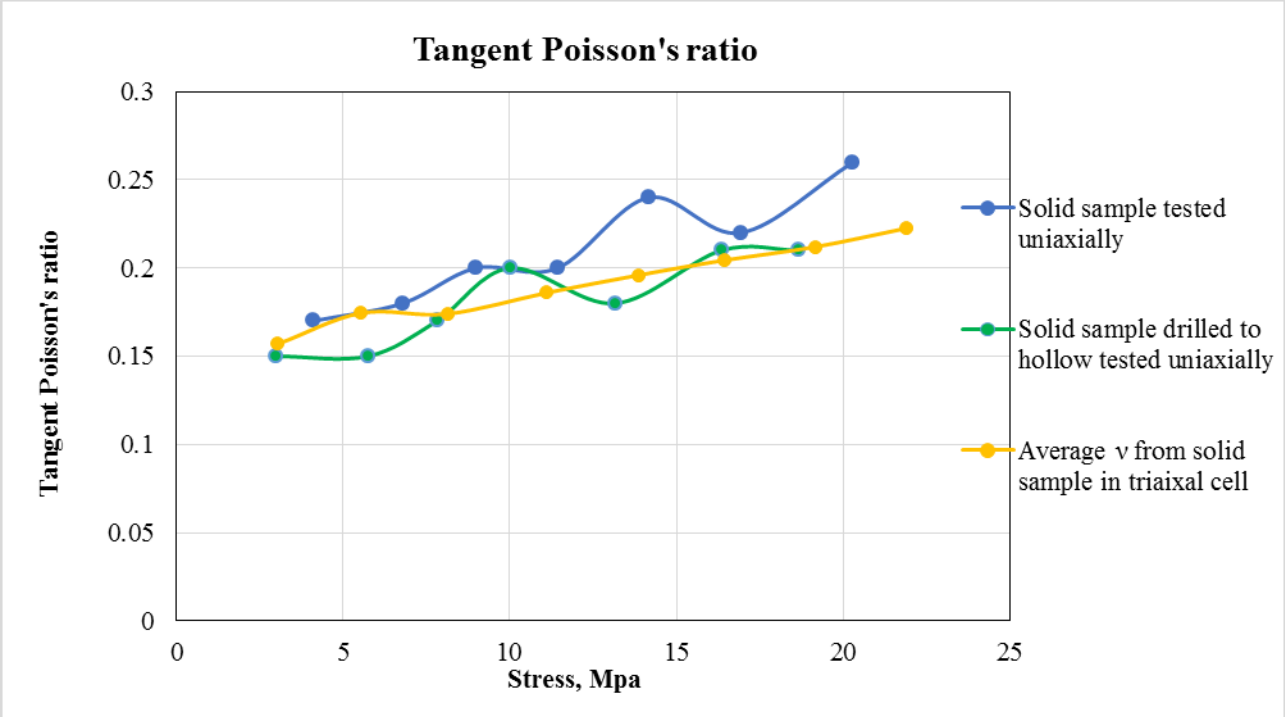

Figure 5. Comparison of mean tangent Poisson's ratios from a solid sample tested uniaxially in a triaxial cell and uniaxially in a universal test machine. Also shown is the results of re-testing in the universal test machine after drilling the sample with an axial 26 mm hole to represent an overcore sample.

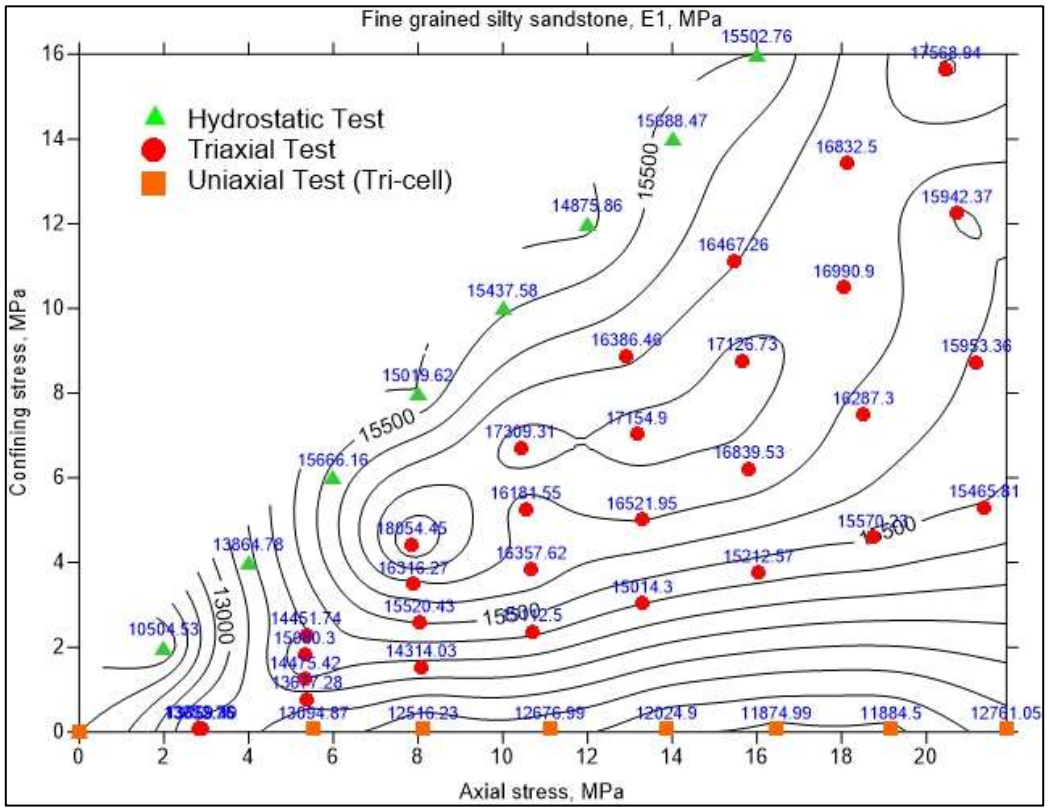

Figure 6. Isopach of E_1 with respect to axial and confining stress

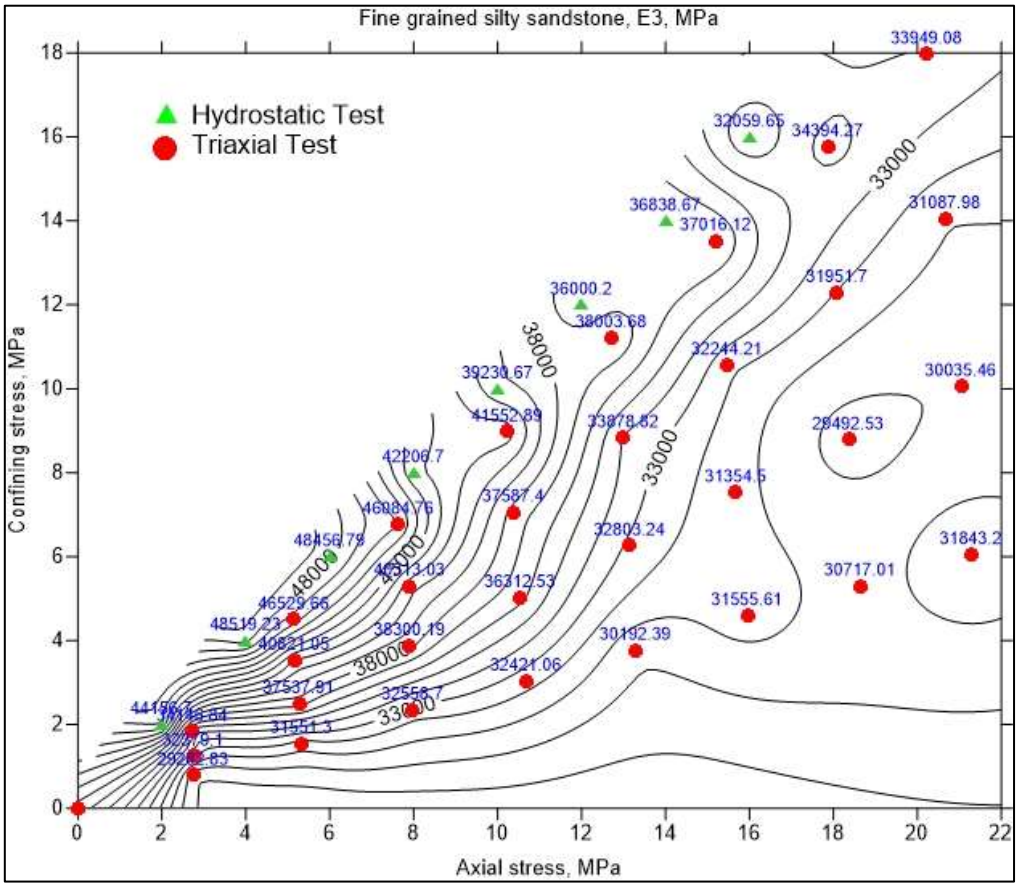

Figure 7. Isopach of E_3 with respect to axial and confining stress

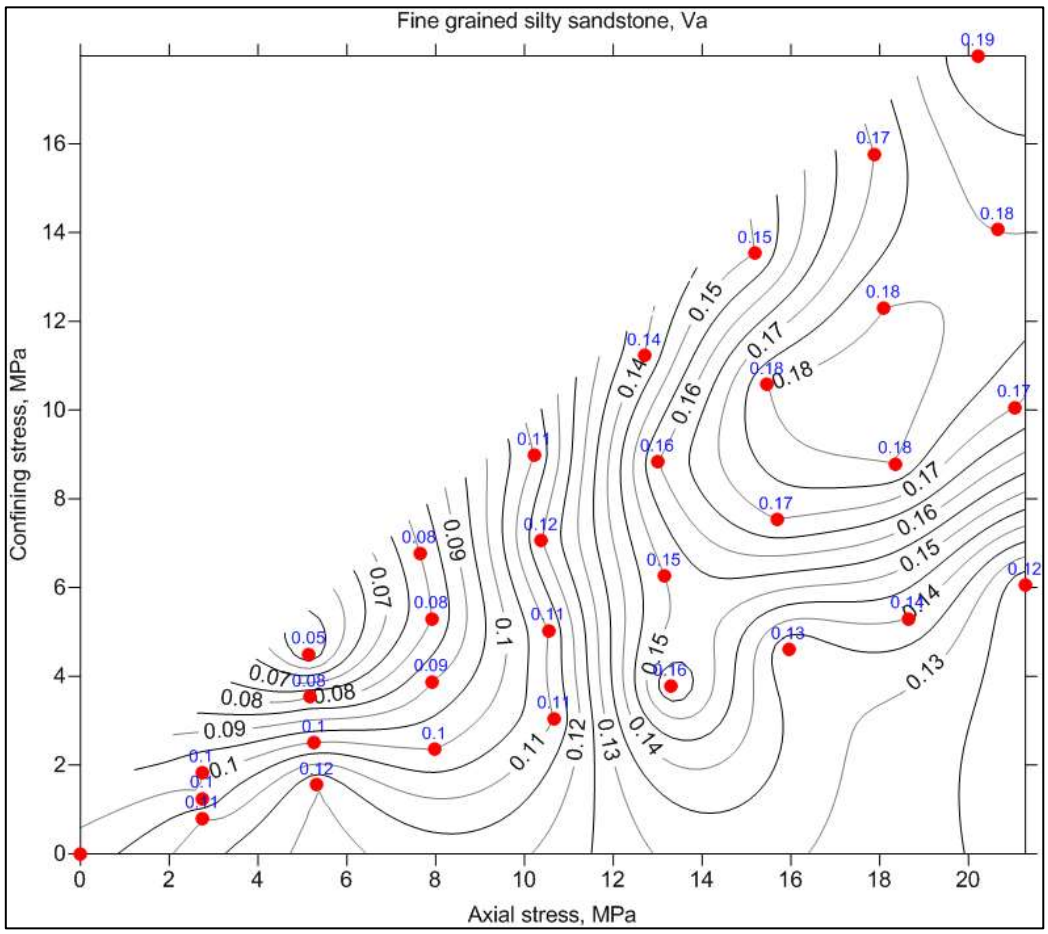

Figure 8. Isopach of v_a with respect to axial and confining stress

3.2 A porous sandstone

Another sample tested was a porous Hawkesbury sandstone from the Sydney area. This sample was of particular interest because of the change in Young's moduli associated with stress and because it exhibited significant poroelastic effects.

Figure 9 shows the axial Young's modulus of the sample. This varies from 4.2 GPa at low stress to 16.2 GPa at an axial stress of 21 MPa and a confining stress of 12 MPa. The near vertical isopachs indicate that the axial Young's modulus is primarily dependent on the axial stress.

Figure 10 shows the major transverse modulus of the sample. This varies from 3.6 GPa at low stress to 18.4 GPa at a confining stress of 18 MPa. The near horizontal isopachs indicate that the horizontal Young's modulus is dependent on confining stress. In this sample the minor horizontal Young's modulus was similar to the major one.

The Poisson's ratio, v_{13}, is shown for the sample in Figure 11. This shows low values of less than 0.1 for near equal axial and confining stress. With increasing differences between these two stresses leading to shear stress, this value increases to nearly 0.25. Figure 13 shows this behaviour in more detail. It shows the value of Poisson's ratio from the uniaxial test and triaxial test with different levels of confining stress respectively. The uniaxial loading case shows a tangent Poisson's ratio that reaches 0.5 at 17 MPa axial load. Poisson's ratio is lower when the confining pressure is higher, which means lower shear stress.

The poroelastic behaviour for effective stress in the axis of the sample is shown in Figure 12. It shows values of the axial poroelastic coefficient that are lowest (0.5~0.6) where axial and confining stress are approximately equal and increase with increasing shear stress (0.75).

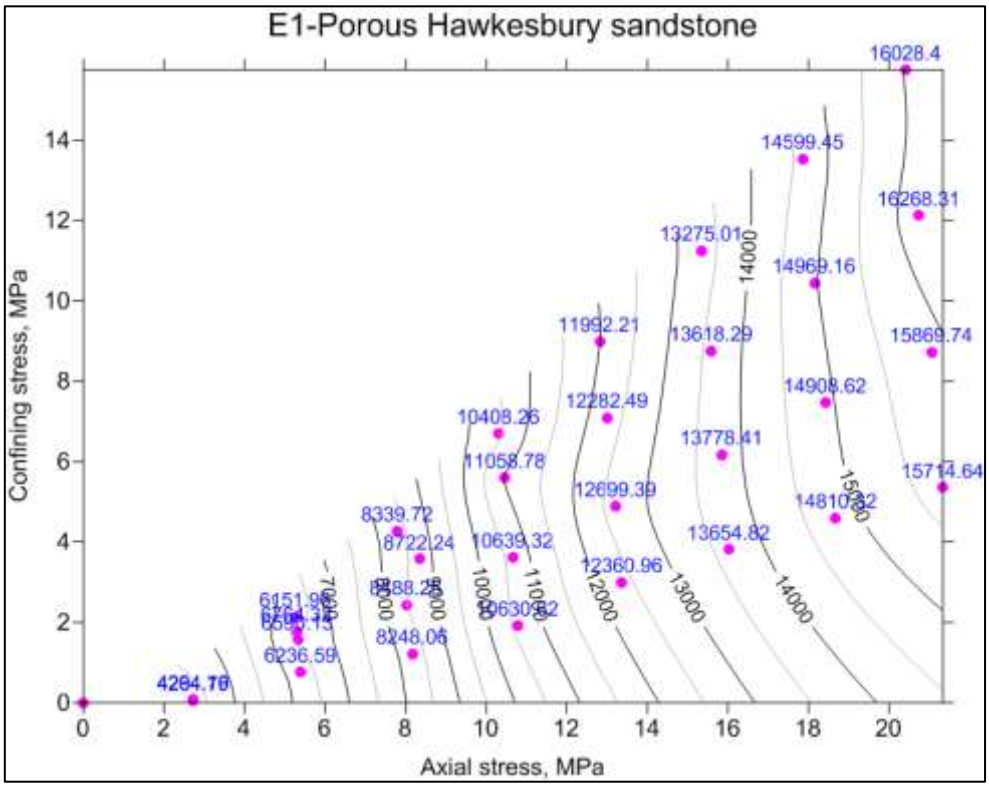

Figure 9. Axial Young's modulus from a porous sandstone

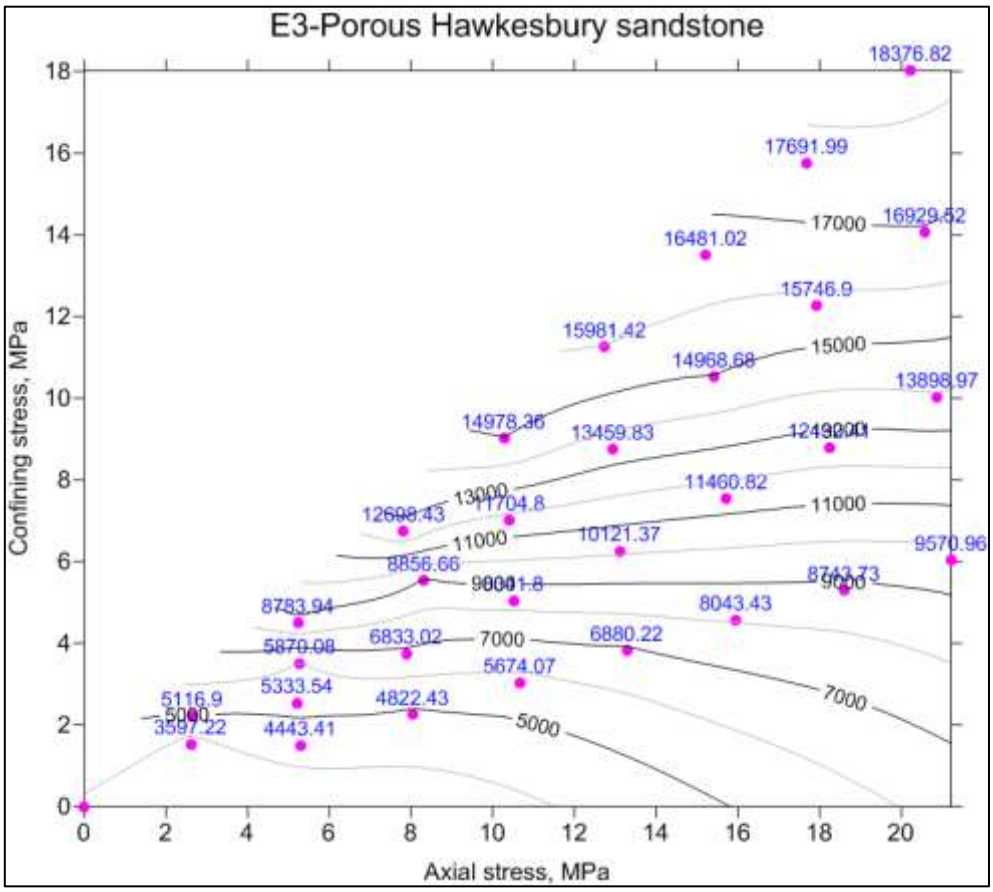

Figure 10. Major transverse modulus from a porous sandstone

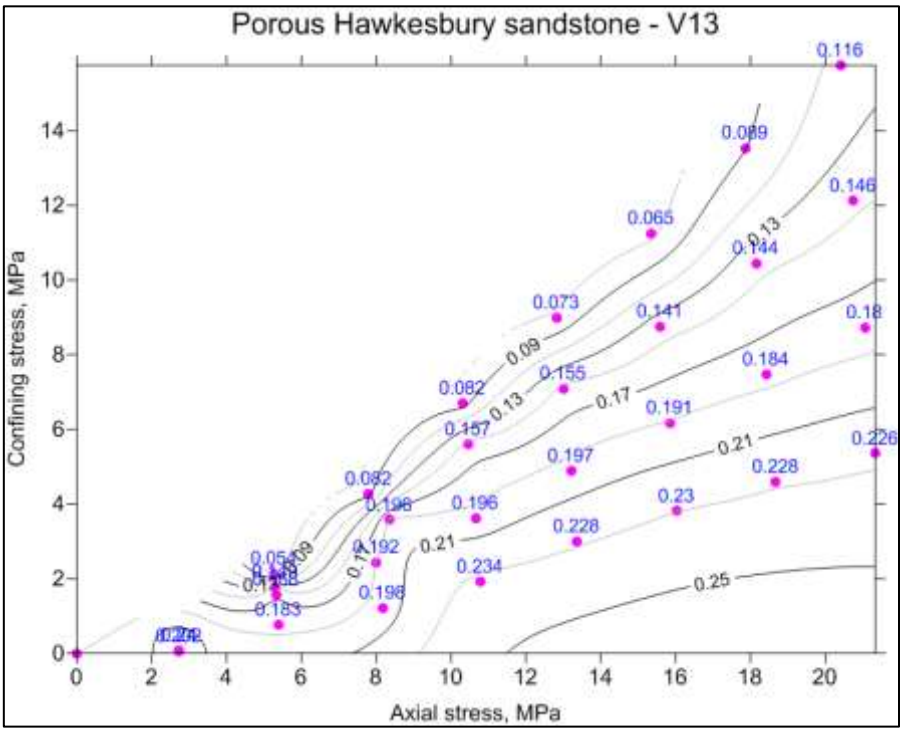

Figure 11. Poisson's ratio, v_{13}, from a porous sandstone

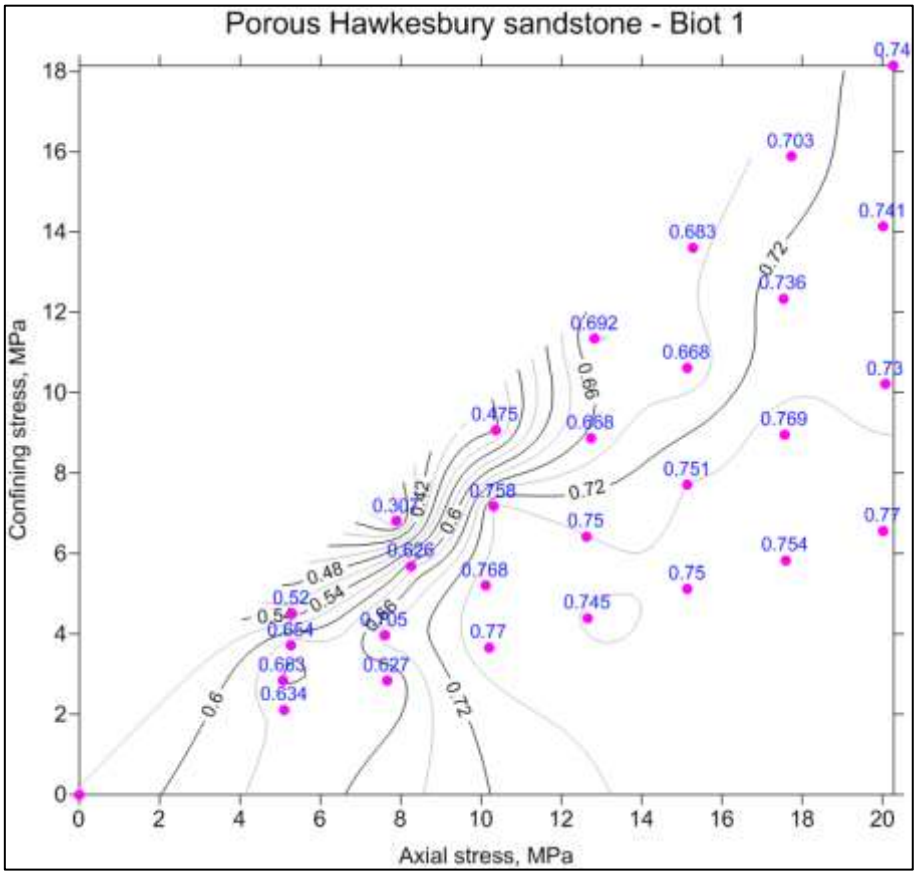

Figure 12. Poroelastic coefficient in axial direction from a porous sandstone

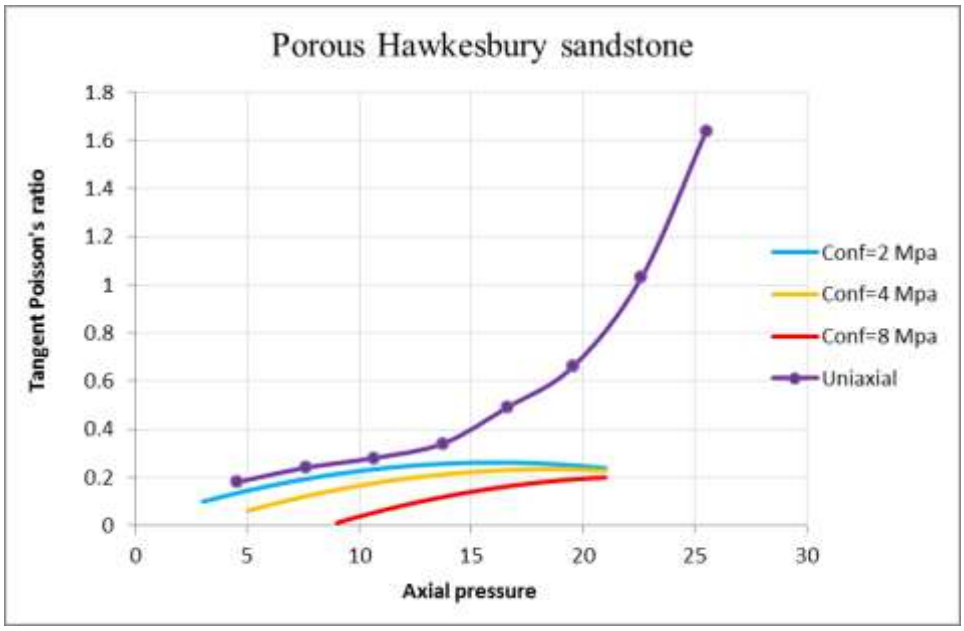

Figure 13. Plot of Poisson's ratio, $v_{13,}$ showing increase with shear stress

4. Conclusions

This paper has presented an approach to obtain the orthotropic elastic parameters from triaxial and hydrostatic loading of core and rock fragments respectively. This does not mean that the rock necessarily behaves in an orthotropic manner. Rather it is an improved approximation to the usual case where isotropic behaviour is assumed. This paper also presents a means by which the poroelastic behaviour of the rock may be determined within the framework of orthotropic parameters. Orthotropic parameters are within the range of most finite element analysis techniques while cases of fully anisotropic behaviour are generally not yet accommodated.

Experimentally two sedimentary rock samples have been tested. The first is a fine grained, laminated, silty sandstone. This exhibits minor nonlinearity but does show a high degree of anisotropy. The transverse stiffness (parallel with the bedding planes) is approximately 2 to 3 times the axial stiffness. The sample exhibited a fairly low value of the geometric mean Poisson's ratio that increases with stress. The individual values of Poisson's ratios vary quite widely as a function of the anisotropy of the sample. The sample exhibited negligible poroelastic effects.

The second set of experimental results comes from a test on a medium grained sample of porous Hawkesbury sandstone. It was relatively isotropic but was very nonlinearly elastic with Young's modulus changes of 4.5:1 within a 20 MPa stress range. It also had a lower value of Poisson's ratio except under uniaxial loading conditions. In the latter case the value of Poissons's ratio increased rapidly with stress. This is quite a common feature of a number of sedimentary rocks.

The benefits of the hydrostatic test method are many. It is simple to test quite small pieces of rock such as 10 mm cubes, or those of less regular geometry. Its limitation is in the need to estimate the mean value of Poisson's ratio to be able to get a suitable solution. Even with this limitation the benefit of being able to compare the ratio of principal Young's moduli is considerable.

References

Gray, I., Wood, J.H. and Shelukina, I, 2013, Real Stress Distributions in Sedimentary Strata. Proceedings of the 6th International Symposium on In-Situ Rock Stress, International Society for Rock Mechanics, Sendai, Japan, 20-22 August 2013.

Gray, I., 2017, Effective Stress in Rock. Deep Mining 2017: Eighth International Conference on Deep and High Stress Mining – J Wesseloo (ed.) 2017. Australian Centre for Geomechanics, Perth, ISBN 978-0-9924810-6-3.

Huber, M., 1923, The theory of crosswise reinforced ferroconcrete slabs and its application to various important constructional problems involving concrete slabs. Der Bauingenieur 4, 12 (1923), 354–360. 4.